

# Integrable Hamiltonian systems with swallowtails

K Efstathiou<sup>1</sup> and D Sugny<sup>2</sup>

<sup>1</sup> Johann Bernoulli Institute for Mathematics and Computer Science, University of Groningen, PO Box 407, 9700AK Groningen, The Netherlands

<sup>2</sup> Institut Carnot de Bourgogne, UMR 5209 CNRS, Université de Bourgogne, BP 47870, 21078 Dijon, France

E-mail: [K.Efstathiou@rug.nl](mailto:K.Efstathiou@rug.nl) and [dominique.sugny@u-bourgogne.fr](mailto:dominique.sugny@u-bourgogne.fr)

Received 21 August 2009, in final form 23 December 2009

Published 8 February 2010

Online at [stacks.iop.org/JPhysA/43/085216](http://stacks.iop.org/JPhysA/43/085216)

## Abstract

We consider two-degree-of-freedom integrable Hamiltonian systems with bifurcation diagrams containing swallowtail structures. The global properties of the action coordinates in such systems together with the parallel transport of the period lattice and corresponding quantum cells in the joint spectrum are described in detail. The relation to the concept of bidromy which was introduced in Sadovskii and Zhilinskiĭ (2007 *Ann. Phys.* **322** 164–200) is discussed.

PACS number: 45.20.Jj

(Some figures in this article are in colour only in the electronic version)

## 1. Introduction

Consider a Liouville integrable Hamiltonian system on a four-dimensional manifold  $N$  with the symplectic form  $\omega$ . The dynamics of the system is given by the Hamiltonian function  $H : N \rightarrow \mathbf{R}$  which defines the Hamiltonian vector field  $X_H$  through the relation  $\omega(X_H, \cdot) = dH$ . Integrability means that there is a second function  $J : N \rightarrow \mathbf{R}$  which is an integral of  $X_H$ , i.e.  $X_H(J) = \{J, H\} = \omega(X_J, X_H) = 0$ , and such that  $H$  and  $J$  are almost everywhere linearly independent. The latter condition means that the rank of the derivative  $DF(x)$  of the *integral map*

$$F : N \rightarrow \mathbf{R}^2 : x \mapsto F(x) = (H(x), J(x)) \quad (1)$$

is maximal for almost all  $x \in N$ .

Let  $f \in \mathbf{R}^2$  be an element of the image of  $F$  and consider the *fiber*  $F^{-1}(f)$ . If  $DF(x)$  has maximal rank for all  $x \in F^{-1}(f)$ ,  $f$  is a *regular value*; otherwise, it is *critical*. By the Arnol'd–Liouville theorem, if  $f$  is a regular value,  $F^{-1}(f)$  is a smooth torus  $\mathbf{T}^2$  or a union of

such tori. This type of information is encoded in the bifurcation diagram  $\mathcal{BD}$ ; all the elements of the image of  $F$  are depicted in the  $\mathcal{BD}$  and for each value  $f \in \text{image}(F) \subseteq \mathbf{R}^2$ , the  $\mathcal{BD}$  shows whether  $f$  is regular or critical, and the type of the fiber  $F^{-1}(f)$ .

Denote by  $\mathbf{R} \subseteq \mathbf{R}^2$  a connected set of regular values of  $F$ . The preimage  $F^{-1}(\mathbf{R})$  is a  $\mathbf{T}^2$  fiber bundle over  $\mathbf{R}$ . Smooth action-angle coordinates can be defined in any simply connected subset of  $\mathbf{R}$ . When  $\mathbf{R}$  is not simply connected because, for example, there are critical values in the interior of  $\text{image}(F)$ , it is possible that smooth action-angle coordinates cannot be defined globally, i.e., in the entire  $\mathbf{R}$  [1, 2]. The basic topological obstruction to the existence of global actions is non-trivial *monodromy* of the  $\mathbf{T}^2$  fiber bundle over  $\mathbf{R}$ , see [2]. In quantum systems non-trivial monodromy signifies the absence of good quantum numbers; for the general theory and examples, see [3–5].

The existence of non-trivial monodromy can be detected by the parallel transport of a basis of the first homology group  $H_1(\mathbf{T}^2(f), \mathbf{Z})$  of the regular fiber  $\mathbf{T}^2(f) = F^{-1}(f)$  for  $f \in \mathbf{R}$  along a closed path  $\Gamma$  that lies entirely in  $\mathbf{R}$  and is not homotopic to a point in  $\mathbf{R}$  [2]. The linear transformation  $M_\Gamma \in \text{GL}(2, \mathbf{Z})$ <sup>3</sup> that connects the initial and final bases of  $H_1(\mathbf{T}^2(f), \mathbf{Z})$  is called the *monodromy matrix* and is the same for all homotopic paths  $\Gamma$  in  $\mathbf{R}$ . The system has non-trivial monodromy, and thus no global action-angle coordinates, when  $M$  is *not* the identity matrix at least for one closed path  $\Gamma$ .

This standard notion of monodromy has been recently generalized to fractional monodromy [6–12]. The main difference between standard and generalized monodromy is that, in the latter, the path  $\Gamma$  crosses a line  $\mathcal{C}$  of critical values of  $F$  that correspond to *curled tori*, see [8]. Thus in fractional monodromy our interest is not restricted to the fibration of the phase space over the set  $\mathbf{R}$  of regular values of  $F$  but is extended to include also sets of critical values of  $F$ . Furthermore, this leads naturally to the question of the behavior of the action variables near the line  $\mathcal{C}$  of critical values of  $F$  [11, 13].

Another generalized monodromy, called *bidromy*, was proposed in [14]. Bidromy was introduced in the example of a three-degree-of-freedom (3-DOF) integrable Hamiltonian system but its defining characteristics can be studied in 2-DOF systems with  $\mathcal{BD}$  that contains a swallowtail. The main motivation of our work is thus to study such systems, analyze the qualitative properties of their fibration, study the properties of the action coordinates and relate our results to the concept of bidromy. We make further comments on bidromy after we describe the setting of our paper.

We would like to emphasize here that we adopt a ‘global’ point of view. Integrable 2-DOF Hamiltonian systems with bitori have been studied before, see for example [15–17]. Nevertheless, such studies are ‘local’ in the sense that they describe the neighborhood of a single bitorus or the fibration of a single energy level set. Here we are interested on the consequences of the whole one-parameter family of bitori on the qualitative properties of the system. The assumption that the system has a swallowtail is from this point of view a ‘global’ assumption that describes how the one-parameter family of bitori is embedded in the complete fibration.

This work is part of a research program that aims to understand the Lagrangian torus fibration of the phase space of integrable Hamiltonian systems with codimension-1 hyperbolic singularities. Note that both curled tori and bitori are codimension-1 hyperbolic periodic orbits together with their stable and unstable manifolds. Such singular fibers form, in 2-DOF systems, 1-parameter families that locally separate the phase space. For a long time it was thought that such families formed impenetrable ‘walls’ and that it did not make sense to connect the two parts of the phase space at each side of this ‘wall’. The introduction of

<sup>3</sup>  $\text{GL}(2, \mathbf{Z})$  is the group of  $2 \times 2$  integer matrices with the determinant  $\pm 1$ .

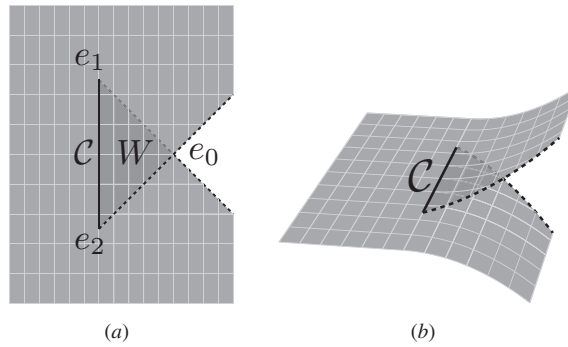


**Figure 1.** (a) Schematic representation of the bifurcation diagram  $\mathcal{BD}$  in the neighborhood  $U$  of the two-component region, and (b) the unfolded bifurcation diagram  $\overline{\mathcal{BD}}$ .

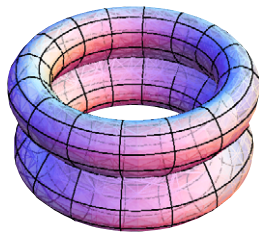


**Figure 2.** The bitorus consists of two tori that are glued along a single circle. Dynamically, the circle is a hyperbolic periodic orbit. The stable and unstable manifolds of this orbit coincide and consist of two disconnected components. The closure of each of these components corresponds to one of the two tori that are glued together to form the bitorus.

(This figure is in colour only in the electronic version)

*fractional monodromy* [6–9, 12, 13, 18, 19] and *bidromy* [14] shows that this is not the case, and that it is possible to establish connections between the two parts of the phase space locally separated by these ‘walls’ by the continuation of, in the classical case, homology cycles or, in the quantum case, elementary cells through the ‘walls’. In the present work we describe in detail the properties of the fibration for systems with bidromy. An outlook of further research along these lines for more complicated arrangements of codimension-1 singularities is given in section 4.

In this paper, we consider 2-DOF integrable Hamiltonian systems  $F = (H, J)$  defined on the symplectic manifold  $(N, \omega)$ , such that the image of  $F$  contains a neighborhood  $U$ , in which

- (i) the  $\mathcal{BD}$  has the swallowtail structure depicted in figure 1(a) and
- (ii) the flow of the Hamiltonian vector field  $X_J$  defines a free  $\mathbf{S}^1$  action in  $F^{-1}(U)$ .

We describe now in detail the swallowtail structure depicted in figure 1(a). The open (in  $U$ ) set  $W$  of the swallowtail (dark gray in figure 1(a)) consists of regular values  $f$  of the integral map  $F$  for which the preimage  $F^{-1}(f)$  is the disjoint union of two smooth tori  $\mathbf{T}^2$ . We denote the two tori by  $\mathbf{T}_+^2(f)$  and  $\mathbf{T}_-^2(f)$ . For points  $f$  on the thick black curve  $\mathcal{C}$  (which does not include the endpoints  $e_1, e_2$ ), the preimage  $F^{-1}(f)$  is a bitorus  $\text{bi}\mathbf{T}^2(f)$ , depicted in figure 2. We can think of  $\text{bi}\mathbf{T}^2(f)$  as the tori  $\mathbf{T}_+^2(f)$  and  $\mathbf{T}_-^2(f)$  joined together along an  $X_J$  orbit. At the dashed curve  $e_0e_1$  the torus  $\mathbf{T}_-^2(f)$  degenerates to a circle  $\mathbf{S}^1(f)$  while the torus

$\mathbf{T}_+^2(f)$  can be continued through the dashed curve. At the second dashed curve  $e_0e_2$ , it is  $\mathbf{T}_+^2(f)$  that degenerates to a circle  $\mathbf{S}_+^1(f)$  while  $\mathbf{T}_-^2(f)$  can be continued through the corresponding curve. Concrete examples of 2-DOF integrable Hamiltonian systems with such swallowtail structure in their  $\mathcal{BD}$  are given in section 3.

**Remark 1.** In the swallowtail structure, the number of connected components of the fibers is not constant. Other integrable Hamiltonian systems have the same property but do not have bidromy. For a simple example see the quadratic spherical pendulum [20]. For a similar situation in a non-Hamiltonian context, see [21–23].

It is often useful to use, instead of the  $\mathcal{BD}$ , the concept of the *unfolded bifurcation diagram*  $\overline{\mathcal{BD}}$  where each point corresponds to exactly one connected component of the fibration, see [7, 24]; compare also with the concept of a local bifurcation diagram [25].

**Definition 1.** *The unfolded bifurcation diagram  $\overline{\mathcal{BD}}$  is a pathwise connected set together with a continuous projection  $\pi : \overline{\mathcal{BD}} \rightarrow \mathcal{BD}$  such that for each  $f \in \mathcal{BD}$ , the number of points in  $\pi^{-1}(f) \subset \overline{\mathcal{BD}}$  is equal to the number of connected components of  $F^{-1}(f)$ ; thus, each point  $\bar{f} \in \overline{\mathcal{BD}}$  corresponds to exactly one connected component of  $F^{-1}(f)$ .*

The unfolded bifurcation diagram  $\overline{\mathcal{BD}}$  for the swallowtail is depicted schematically in figure 1(b). We denote by  $\bar{\mathcal{R}}$  the set of points  $\bar{f} \in \overline{\mathcal{BD}}$  that lift to a smooth two-dimensional torus  $\mathbf{T}^2(\bar{f})$  in phase space. For each  $f \in W$ , there are two points  $\bar{f}^+$  and  $\bar{f}^-$  in  $\overline{\mathcal{BD}}$  such that  $\pi(\bar{f}^+) = \pi(\bar{f}^-) = f$  and  $\mathbf{T}_\pm^2(f) = F^{-1}(\bar{f}^\pm)$ . Thus, the set  $W \subset \mathcal{BD}$  lifts under  $\pi^{-1}$  to two sets  $W_+, W_- \subset \overline{\mathcal{BD}}$ .

Since  $X_J$  defines an  $\mathbf{S}^1$  action in  $F^{-1}(U)$ , the function  $J$  is a globally defined action variable<sup>4</sup>. Note that  $J$  and  $X_J$  are smooth on the whole  $\mathcal{BD}$  including the set of critical values of  $F$ . Furthermore  $\bar{\mathcal{R}}$  is simply connected. Thus it is possible to define a second action variable  $I$  in the entire  $\bar{\mathcal{R}}$ , i.e. in  $\mathcal{BD}$  excluding  $\mathcal{C}$ . We always choose  $I$  so that the Hamiltonian vector fields  $X_J$  and  $X_I$  form a basis of the period lattice [2], i.e. all other Hamiltonian vector fields corresponding to actions can be expressed as integral combinations of  $X_J$  and  $X_I$ . Furthermore,  $J$  is special since it is globally defined and for this reason we keep it fixed in our considerations. These two requirements in the choice of  $I$  imply that  $X_I$  is defined up to a sign and an integer multiple of  $X_J$ , i.e. if  $X_I$  satisfies the above requirements, then so does  $\pm X_I + kX_J$  with  $k \in \mathbf{Z}$ . The only relevant question concerning  $I$  is whether its values at the two sides of  $\mathcal{C}$  ‘match’ since as we show below it is only in this case that the corresponding homology cycle can be continued through  $\mathcal{C}$ . In order to facilitate the discussion, we define the following class of paths on  $\mathcal{BD}$ .

**Definition 2.** *A  $\mathcal{C}$ -crossing path is a path  $\Gamma : [0, 1] \rightarrow \mathcal{BD}$  that crosses  $\mathcal{C}$  transversally at a point  $c = \Gamma(t_c)$  with  $t_c \in (0, 1)$ .*

Consider a  $\mathcal{C}$ -crossing path  $\Gamma$  and assume that for  $t < t_c$ ,  $\Gamma(t) \notin W$  while for  $t > t_c$ ,  $\Gamma(t) \in W$ . Then for  $t > t_c$ , let  $\Gamma_+(t) \in W_+$  and  $\Gamma_-(t) \in W_-$ , see figure 3.

**Definition 3.** *The smooth action  $I$  defined on  $\bar{\mathcal{R}}$  is good if*

$$\lim_{t \rightarrow t_c^-} I(\Gamma(t)) = \lim_{t \rightarrow t_c^+} \Sigma I(\Gamma(t)) := \lim_{t \rightarrow t_c^+} (I(\Gamma_+(t)) + I(\Gamma_-(t))),$$

for all  $\mathcal{C}$ -crossing paths  $\Gamma$ .

<sup>4</sup> By ‘global’ in this paper we refer to quantities defined in the whole of  $F^{-1}(U)$ .

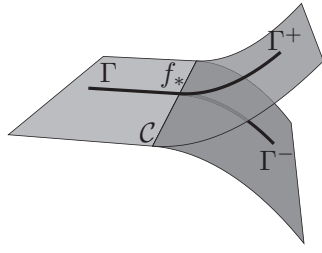


**Figure 3.** The path  $\Gamma$  splits into two parts  $\Gamma^+$  and  $\Gamma^-$  in  $\overline{\mathcal{BD}}$  as it enters the double-component region.

As we show in section 2, if  $I$  is a smooth action defined on  $\bar{\mathbb{R}}$  then

$$\lim_{t \rightarrow t_c^-} I(\Gamma(t)) - \lim_{t \rightarrow t_c^+} \Sigma I(\Gamma(t)) = kJ(\Gamma(t_c)) + l,$$

for some  $k \in \mathbb{Z}$  and  $l \in \mathbb{R}$  that do not depend in any way on  $\Gamma(t)$ . Therefore,  $I$  is good when  $k = l = 0$ . But then note that for the action  $I' = I + kJ + l$ , we have

$$\lim_{t \rightarrow t_c^-} I'(\Gamma(t)) - \lim_{t \rightarrow t_c^+} \Sigma I'(\Gamma(t)) = 0.$$

Thus we obtain the following result.

**Theorem 1.** *Integrable two-degree-of-freedom Hamiltonian systems with a swallowtail have a unique (up to a sign) good action  $I_0$  defined in a neighborhood of  $\mathcal{C}$  which is open in  $\bar{\mathbb{R}}$ .*

As we already mentioned, the original motivation for this work has been the paper [14] in which the concept of *bidromy* was introduced. The integrable Hamiltonian system described in section 3.2 is derived from the three-degree-of-freedom Hamiltonian system studied in [14]. Bidromy in [14] is found in the joint quantum spectrum of this 3-DOF system but it is also described in terms of the parallel transport of homology cycles along a *bipath*. The  $\mathcal{BD}$  of this 3-DOF system contains a region of regular values  $f$  for which  $F^{-1}(f)$  consists of two connected components  $\mathbf{T}^3$ , see [14] for more details. The essence of this structure is preserved in the two-degree-of-freedom system studied in section 3.2, where we have the swallowtail structure described above. We show that it is always possible to find a basis of an appropriate subgroup of  $H_1(\mathbf{T}^2(f), \mathbb{Z})$  in which the transformation of the basis along a bipath is as trivial as possible. In particular, one of the elements of the basis remains invariant while the second one is doubled. An analogous result holds for the parallel transport of quantum cells in the joint spectrum along the bipath. The existence of such homology basis and corresponding quantum cell are the consequence of the existence of a unique *good* action in the system.

We give a brief overview of the paper. In section 2, we study action coordinates in the neighborhood of the line of critical values  $\mathcal{C}$ . Furthermore, we relate these action coordinates to the parallel transport of homology cycles and quantum elementary cells, and to the notion of the rotation number. In section 3, we study two examples of 2-DOF integrable Hamiltonian systems with swallowtails. We describe in detail the parallel transport of quantum cells and their continuation through  $\mathcal{C}$ . In particular, the 2-DOF system studied in section 3.2 is the reduction of the 3-DOF system studied in [14] and we use it in order to discuss in a simpler context the results of [14] on bidromy. We conclude in section 4 with a discussion of our results.

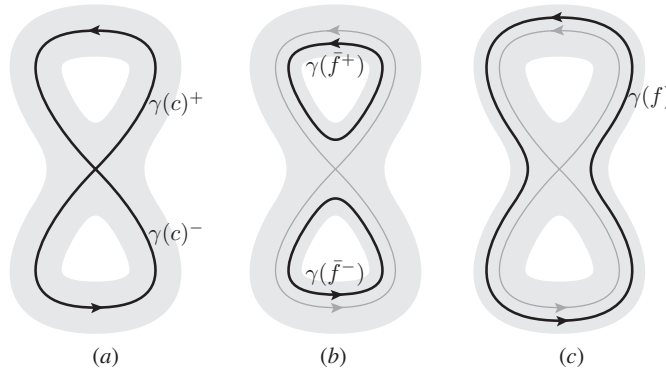


**Figure 4.** Intersection of the fibers  $F^{-1}(f)$  with the Poincaré surface of section  $\Sigma$ . (a) For  $f = c \in \mathcal{C}$  the intersection  $\gamma_c$  of  $F^{-1}(c)$  with  $\Sigma$  is a figure-8 that consists of the two parts  $\gamma(c)^+$  and  $\gamma(c)^-$ . (b) For  $f \in W$  near  $\mathcal{C}$  the fiber  $F^{-1}(f)$  consists of two connected components  $\mathbf{T}_+^2(f)$  and  $\mathbf{T}_-^2(f)$  with respective intersections with  $\Sigma$ ,  $\gamma^+(f)$  and  $\gamma^-(f)$ . (c) For  $f$  near  $\mathcal{C}$  but outside  $W$  the fiber  $F^{-1}(f)$  consists of a single connected component  $\mathbf{T}^2(f)$  with intersection  $\gamma(f)$  with  $\Sigma$ .

## 2. Action coordinates and parallel transport of homology cycles

In this section we consider systems with a swallowtail as described in section 1. We show the existence of a unique good action in  $\bar{\mathbb{R}}$  and we study the parallel transport of homology cycles and their continuation through the curve  $\mathcal{C}$  of bitori.

### 2.1. Local structure of the fibration and homology cycles near $\mathcal{C}$

The structure of the fibration near  $\mathcal{C}$  is most easily described if we consider a Poincaré section  $\Sigma$  for the flow of  $X_J$  restricted to a level set  $J^{-1}(j)$ . Consider a  $\mathcal{C}$ -crossing curve  $f_t = \Gamma(t)$  for  $t \in [0, 1]$  with constant value  $J = j$  along  $\Gamma$  such that  $f_0 = \Gamma(0) \notin W$  and  $f_1 = \Gamma(1) \in W$  (so  $\Gamma$  starts outside  $W$ , crosses  $\mathcal{C}$  and ends inside  $W$ ), see figure 3.

Recall that points on  $\mathcal{C}$  lift in phase space to bitori  $\text{bi}\mathbf{T}^2$ . These can be viewed as two topological tori  $\mathbf{T}^2$  glued together along an  $X_J$  orbit or, alternatively, as the Cartesian product of a figure-8 with a circle  $\mathbf{S}^1$ . The intersection of  $\text{bi}\mathbf{T}^2$  with the Poincaré section  $\Sigma$  is the figure-8  $\gamma(c)$  depicted in figure 4(a). The whole fiber  $\text{bi}\mathbf{T}^2$  can be reconstructed by considering all  $X_J$  orbits that start at points  $p \in \gamma(c)$  and come back to  $p$  after time  $2\pi$  which implies that the fiber  $\text{bi}\mathbf{T}^2$  is the product  $\gamma(c) \times \mathbf{S}^1$ . For  $f$  in the double component region  $W$ , the fiber  $F^{-1}(f)$  consists of two smooth two-dimensional tori  $\mathbf{T}^2(\bar{f}^+) = F^{-1}(\bar{f}^+)$  and  $\mathbf{T}^2(\bar{f}^-) = F^{-1}(\bar{f}^-)$ . The intersection of each of the components  $\mathbf{T}^2(\bar{f}^\pm)$  with  $\Sigma$  is in this case a smooth circle  $\gamma(\bar{f}^\pm)$ , see figure 4(b). For  $f$  close to  $\mathcal{C}$  but outside  $W$  the fiber  $F^{-1}(f) = F^{-1}(\bar{f})$  is the torus  $\mathbf{T}^2(\bar{f})$  and its intersection with  $\Sigma$  is the smooth circle  $\gamma(\bar{f})$ , see figure 4(c). Thus as  $t \rightarrow t_c^-$ , we obtain on  $\Sigma$  a family of circles  $\gamma(\bar{f}_t)$  that approaches the figure-8  $\gamma(c)$ . On the other hand, we have that as  $t \rightarrow t_c^+$  the families  $\gamma(\bar{f}_t^+)$  and  $\gamma(\bar{f}_t^-)$  approach  $\gamma(c)^+$  and  $\gamma(c)^-$ , respectively. This means that

$$\lim_{t \rightarrow t_c^+} \gamma(\bar{f}_t^+) + \lim_{t \rightarrow t_c^+} \gamma(\bar{f}_t^-) = \gamma(c)^+ + \gamma(c)^- = \lim_{t \rightarrow t_c^-} \gamma(\bar{f}_t).$$

We look now at the first homology group of connected components of fibers of  $F$ . For all toric fibers  $\mathbf{T}^2(\bar{f}) = F^{-1}(\bar{f})$  with intersection  $\gamma(\bar{f})$  with  $\Sigma$  we can take as basis of  $H_1(\mathbf{T}^2(\bar{f}), \mathbf{Z})$  the homology class  $g(\bar{f})$  of  $\gamma(\bar{f})$  and the homology class  $b(\bar{f})$  of any closed

$X_J$  orbit on  $\mathbf{T}^2$ . For  $\text{bi}\mathbf{T}^2 = F^{-1}(c)$ , the first homology group  $H_1(\text{bi}\mathbf{T}^2, \mathbf{Z})$  is generated by the homology class  $b(c)$  of any closed  $X_J$  orbit on  $\text{bi}\mathbf{T}^2$ , and the homology classes  $g(c)^+$  and  $g(c)^-$  of  $\gamma(c)^+$  and  $\gamma(c)^-$ , respectively. From the previous discussion on the behavior of the intersections  $\gamma$  as  $t \rightarrow t_c$ , we conclude that

$$\lim_{t \rightarrow t_c^+} g(\bar{f}_t^+) + \lim_{t \rightarrow t_c^+} g(\bar{f}_t^-) = g(c)^+ + g(c)^- = \lim_{t \rightarrow t_c} g(f_t). \tag{2}$$

On the other hand, for the cycle  $b$  generated by the flow of  $X_J$ , we have that

$$\lim_{t \rightarrow t_c^+} b(\bar{f}_t^+) = \lim_{t \rightarrow t_c^+} b(\bar{f}_t^-) = \lim_{t \rightarrow t_c} b(\bar{f}_t). \tag{3}$$

Furthermore, we have the following result.

**Lemma 1.** *Let  $V, V_+$  and  $V_-$  be open neighborhoods in  $\bar{\mathbf{R}} \setminus W, W_+$  and  $W_-$ , respectively, so that the boundary of each of these neighborhoods contains the same subset  $\ell$  of  $\mathcal{C}$ . Let  $c \in \ell$ , and consider a  $\mathcal{C}$ -crossing path  $\Gamma$  with  $\Gamma(t) = f_t$  such that  $\bar{f}_0 = \Gamma(0) \in V, \bar{f}_1^+ = \Gamma^+(1) \in W_+, \bar{f}_1^- = \Gamma^-(1) \in W_-$  and  $c = \Gamma(t_c)$  for a unique  $t_c \in (0, 1)$ . Furthermore, let  $I, I_+$  and  $I_-$  be action coordinates defined in  $V, V_+$  and  $V_-$ , respectively, and let  $g, g_+$  and  $g_-$  be the corresponding homology cycles generated by the Hamiltonian flows of these actions. Then we have that*

$$\Delta g(c) := \lim_{t \rightarrow t_c^+} g_+(\bar{f}_t^+) + \lim_{t \rightarrow t_c^+} g_-(\bar{f}_t^-) - \lim_{t \rightarrow t_c} g(\bar{f}_t) = 0, \tag{4}$$

if and only if

$$\Delta I(c) := \lim_{t \rightarrow t_c^+} I_+(\bar{f}_t^+) + \lim_{t \rightarrow t_c^+} I_-(\bar{f}_t^-) - \lim_{t \rightarrow t_c} I(\bar{f}_t) = L, \tag{5}$$

where the constant  $L \in \mathbf{R}$  does not depend on the point  $c \in \ell$ .

**Proof.** The symplectic form  $\omega$  is locally exact in a neighborhood of  $F^{-1}(c)$ , see [15], so there is a 1-form  $\vartheta$  such that locally  $\omega = -d\vartheta$ . Then for the value  $I(\bar{f})$  of the action  $I$  and the corresponding homology cycle  $g(\bar{f})$  on a fiber  $\mathbf{T}^2(\bar{f})$ , we have that

$$I(\bar{f}) = \frac{1}{2\pi} \int_{g(\bar{f})} \vartheta + l,$$

where  $l \in \mathbf{R}$  does not depend on  $\bar{f} \in V$ . A similar relation holds true for  $I_+$  and  $I_-$  but with  $l$  replaced by different constants  $l_+$  and  $l_-$ . Thus by assuming (4) and integrating  $\vartheta$  over the homology cycles  $g, g_+$  and  $g_-$ , we obtain (5).

For the opposite direction, suppose that (5) holds. Then  $\Delta g(c)$  is in general an element of the homology group  $H_1(\text{bi}\mathbf{T}^2(c), \mathbf{Z})$ . Therefore,

$$\Delta g(c) = k_1 g(c)^+ + k_2 g(c)^- + k_3 b(c),$$

for some  $k_1, k_2, k_3 \in \mathbf{Z}$ . Integrating  $\vartheta$  over  $\Delta g(c)$  and taking (5) into account we obtain that

$$k_1 I_+(c) + k_2 I_-(c) + k_3 J(c) = \text{constant},$$

which is true only if  $k_1 = k_2 = k_3 = 0$ . The latter implies (4). This concludes the proof.  $\square$

## 2.2. Parallel transport of homology cycles

In this section we review the most basic facts concerning the parallel transport of homology cycles along (not necessarily closed) paths  $\Gamma$  in the unfolded set  $\bar{\mathbf{R}}$  of regular values of the integral map  $F$ .

The first homology group  $H_1(\mathbf{T}^2(\bar{f}), \mathbf{Z})$  of a regular fiber  $\mathbf{T}^2(\bar{f})$  is isomorphic to the discrete space  $\mathbf{Z}^2$ . The fact that  $H_1(\mathbf{T}^2(\bar{f}), \mathbf{Z})$  is discrete implies that there is a unique notion

of parallel transport of its elements [2]. If we consider two points  $\bar{f}_0$  and  $\bar{f}_1$  in  $\bar{R}$  and a path  $\Gamma : [0, 1] \rightarrow \bar{R}$  connecting these points, then parallel transport of homology cycles defines an isomorphism  $M$  between  $H_1(\mathbf{T}^2(\bar{f}_0), \mathbf{Z})$  and  $H_1(\mathbf{T}^2(\bar{f}_1), \mathbf{Z})$ . This isomorphism  $M$  depends only on the homotopy class of  $\Gamma$ .

If we choose the bases  $(a(\bar{f}_0), b(\bar{f}_0))$  and  $(a(\bar{f}_1), b(\bar{f}_1))$  on  $\mathbf{T}^2(\bar{f}_0)$  and  $\mathbf{T}^2(\bar{f}_1)$  respectively, then the matrix of  $M$  is, in general, an element of  $GL(2, \mathbf{Z})$ . In cases, as in ours, where the set  $\bar{R}$  is orientable it is always possible to choose a consistent orientation for the bases  $(a(\bar{f}_i), b(\bar{f}_i)), i = 1, 2$ . In such a case, the matrix of  $M$  is an element of  $SL(2, \mathbf{Z})$ .

Assume furthermore that, as in our case, the system has a globally defined smooth action  $J$ . The flow of  $X_J$  generates a homology cycle  $b(\bar{f})$  on  $\mathbf{T}^2(\bar{f})$  and thus a smooth family of homology cycles is defined over  $\bar{R}$ . This implies that parallel transport of the homology cycle  $b(\bar{f}_0)$  from  $\bar{f}_0$  to  $\bar{f}_1$  along any path  $\Gamma$  will give the cycle  $b(\bar{f}_1)$ . Consider now on  $\mathbf{T}^2(\bar{f}_0)$  a homology cycle  $a(\bar{f}_0)$  such that  $\{a(\bar{f}_0), b(\bar{f}_0)\}$  is a basis of  $H_1(\mathbf{T}^2(\bar{f}_0), \mathbf{Z})$ . The parallel transport of  $a(\bar{f}_0)$  and  $b(\bar{f}_0)$  to  $\bar{f}_1$  will give the homology cycles  $a'(\bar{f}_1)$  and  $b'(\bar{f}_1)$  that are related to the basis  $\{a(\bar{f}_1), b(\bar{f}_1)\}$  (which has the same orientation as  $\{a(\bar{f}_0), b(\bar{f}_0)\}$ ) of  $H_1(\mathbf{T}^2(\bar{f}_1), \mathbf{Z})$  through an element of  $SL(2, \mathbf{Z})$  as we mentioned before. But furthermore,  $b'(\bar{f}_1) = b(\bar{f}_1)$  and this leaves as the only possibility that  $a'(\bar{f}_1) = a(\bar{f}_1) + kb(\bar{f}_1)$  for some  $k \in \mathbf{Z}$ . This implies that the matrix of the isomorphism  $M$  is

$$\begin{pmatrix} 1 & k \\ 0 & 1 \end{pmatrix}.$$

We close this section with a few remarks on the orientation of the period lattice. It has been remarked in [26] that the orientation of the base space  $\bar{R}$  of the fibration induces an orientation on the fibers and consequently on the period lattice in the following way. Consider a basis  $\{e_1, e_2\}$  of  $T_{\bar{f}}\bar{R}$  and the dual basis  $\{\alpha_1, \alpha_2\}$  of  $T_{\bar{f}}^*\bar{R}$ . Then the vector fields  $X_k, k = 1, 2$ , given by  $\omega(X_k, -) = \alpha_k$  define an orientation on the fiber  $\mathbf{T}^2(\bar{f})$  and its period lattice.

The vectors  $X_J$  and  $X_H$  fix an orientation for all fibres  $\mathbf{T}^2(\bar{f}), \bar{f} \in \bar{R}$ . In the following, we consider this orientation as *positive*. Let  $I$  be an action in our system such that  $X_I$  together with  $X_J$  form a basis of the period lattice at  $\mathbf{T}^2(\bar{f})$ . Since  $I$  is locally a smooth function of  $H$  and  $J$ , i.e. we can write  $I(x) = I(H(x), J(x))$ , we have that

$$X_I = \frac{\partial I}{\partial J} X_J + \frac{\partial I}{\partial H} X_H.$$

It follows that the basis  $\{X_J, X_I\}$  at  $\bar{f}$  is positively (negatively) oriented when  $\partial I / \partial H(\bar{f})$  is strictly positive (respectively negative).

### 2.3. Action coordinates

In this section we study the properties of the second global action  $I$  in  $\bar{R}$ . We start by defining local actions near  $\mathcal{C}$  and then we study how these actions fit together to give an action on  $\bar{R}$ .

In  $\bar{R} \setminus W$  we define a smooth action

$$A(\bar{f}) = \frac{1}{2\pi} \int_{\gamma(\bar{f})} \vartheta, \tag{6}$$

where we have used the fact that  $\omega$  is exact in a neighborhood of  $\mathcal{C}$ , see [15], so there is locally a 1-form  $\vartheta$  such that  $-d\vartheta = \omega$ . When  $N = \mathbf{R}^4$  and  $\omega = dq \wedge dp$  then  $\vartheta = pdq$ . In  $W_+$  and  $W_-$ , we define the actions  $A_+$  and  $A_-$ , respectively, given by

$$A_{\pm}(\bar{f}^{\pm}) = \frac{1}{2\pi} \int_{\gamma(\bar{f}^{\pm})} \vartheta. \tag{7}$$

From the definition of  $A$ ,  $A_+$  and  $A_-$  and from relation (2) we have

$$\lim_{t \rightarrow t_c^+} A_+(\bar{f}_t^+) + \lim_{t \rightarrow t_c^-} A_-(\bar{f}_t^-) = \lim_{t \rightarrow t_c} A(\bar{f}_t). \quad (8)$$

The actions  $A$ ,  $A_+$  and  $A_-$  are smooth univalued functions in their domain of definition. Furthermore note that  $\partial A/\partial H$ ,  $\partial A_{\pm}/\partial H$  are either all strictly positive or all strictly negative depending on the orientation of the integration paths  $\gamma$ ,  $\gamma_{\pm}$  and on whether the value of  $H$  increases or decreases as we approach  $\mathcal{C}$  from inside  $W$ .

Consider now a smooth action  $I$  defined on  $\bar{R}$ . Such an action always exists since  $\bar{R}$  is simply connected. Furthermore since the transformation  $(J, H) \rightarrow (J, I)$  is a local diffeomorphism on  $\bar{R}$  we deduce that  $\partial I/\partial H$  does not change sign. This means that the basis  $(X_I(x), X_J(x))$  of  $T_x\mathbf{T}^2(f)$  has always the same orientation with respect to the basis  $(X_H(x), X_J(x))$ . Then, for any point  $\bar{f}' \in \bar{R} \setminus (W_+ \cup W_-)$ , we have that  $I(\bar{f}') = \sigma' A(\bar{f}') + k' J(\bar{f}') + l'$  with  $\sigma' = \pm 1$  depending on the relative orientation of  $I$  and  $A$ ,  $k' \in \mathbf{Z}$  and  $l' \in \mathbf{R}$ . For  $\bar{f}^{\pm} \in W_{\pm}$  we have in the same way  $I(\bar{f}^{\pm}) = \sigma_{\pm} A_{\pm}(\bar{f}^{\pm}) + k_{\pm} J(\bar{f}^{\pm}) + l_{\pm}$ . Since  $A$ ,  $A_+$  and  $A_-$  are consistently oriented we obtain that  $\sigma = \sigma_+ = \sigma_-$ .

From (8) and the previous discussion, we obtain that

$$\begin{aligned} \lim_{t \rightarrow t_c^+} I(\bar{f}_t^+) - k_+ \lim_{t \rightarrow t_c^+} J(\bar{f}_t^+) - l_+ + \lim_{t \rightarrow t_c^-} I(\bar{f}_t^-) - k_- \lim_{t \rightarrow t_c^-} J(\bar{f}_t^-) - l_- \\ = \lim_{t \rightarrow t_c} I(\bar{f}_t) - \lim_{t \rightarrow t_c} k' J(\bar{f}_t) - l', \end{aligned}$$

or, for  $I' = I + kJ + l$ ,

$$\lim_{t \rightarrow t_c^+} I'(\bar{f}_t^+) + \lim_{t \rightarrow t_c^-} I'(\bar{f}_t^-) - \lim_{t \rightarrow t_c} I'(\bar{f}_t) = (k + k_+ + k_- - k')J(c) + (l + l_+ + l_- - l'). \quad (9)$$

The last equation (9) shows that by choosing  $k = k' - k_+ - k_-$  and  $l = l' - l_+ - l_-$ , we obtain a unique (up to a sign) action  $I_0$  defined in  $\bar{R}$  such that

$$\lim_{t \rightarrow t_c} I_0(\bar{f}_t) = \lim_{t \rightarrow t_c} \Sigma I_0(\bar{f}_t) := \lim_{t \rightarrow t_c^+} I_0(\bar{f}_t^+) + \lim_{t \rightarrow t_c^-} I_0(\bar{f}_t^-). \quad (10)$$

Thus we have proved theorem 1.

We denote by  $g_0(\bar{f})$  the homology cycle generated by the flow of  $X_{I_0}$  on  $\mathbf{T}^2(\bar{f})$ . Equation (10) and lemma 1 imply that

$$\lim_{t \rightarrow t_c^+} g_0(\bar{f}_t^+) + \lim_{t \rightarrow t_c^-} g_0(\bar{f}_t^-) = \lim_{t \rightarrow t_c} g_0(\bar{f}_t). \quad (11)$$

Furthermore, parallel transport of  $g_0(\bar{f}_0)$  to any point  $\bar{f}_1$  along a path  $\Gamma$  that lies entirely in  $\bar{R}$  gives the cycle  $g_0(\bar{f}_1)$ .

#### 2.4. Parallel transport of homology cycles along a bipath and bidromy

In the system with  $\mathcal{BD}$  shown in figure 1(a) there is no non-trivial closed path  $\Gamma$  in the set  $\bar{R}$ . This means that the standard monodromy of the system is trivial. In order to provide a global characterization of the geometry of the fibration near  $\mathcal{C}$  we, following [14], study the parallel transport of homology cycles along a *bipath* on  $\overline{\mathcal{BD}}$ . Such a bipath is shown schematically in figure 5. It consists of two paths that we denote by  $\Gamma_1$  and  $\Gamma_2$ . The path  $\Gamma_1$  starts at the point  $A$  and then crosses  $\mathcal{C}$  at  $B$ . The path continues on  $W^+$  and comes back to  $A$ . The part  $\Gamma_2$  starts also at  $A$ , crosses  $\mathcal{C}$  at  $B$  but then continues on  $W^-$  before coming back to  $A$ .

We begin at  $A$  with the basis  $\{2b(A), g_0(A)\}$  of an index 2 subgroup of  $H_1(\mathbf{T}_A^2, \mathbf{Z})$ , where the cycles  $b$  and  $g_0$  are the cycles generated by the flows of  $X_J$  and the good action  $X_I$ , respectively, as defined in section 2.1. As we approach the point  $B \in \mathcal{C}$  the cycle  $g_0$  approaches a limit that we denote by  $g_0(B)$ . At the other side of  $\mathcal{C}$  (inside  $W$ ) we denote by  $g_0(B^+)$  and

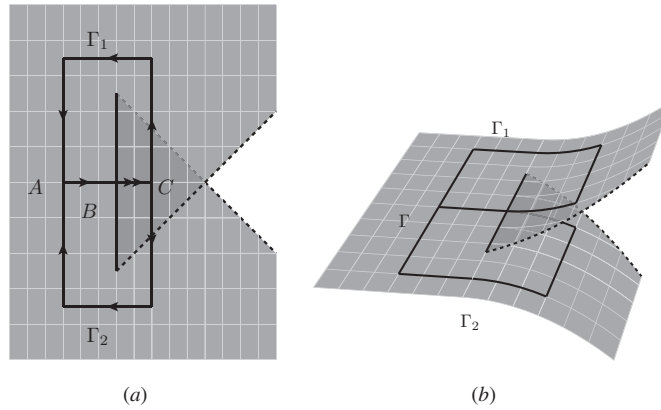


**Figure 5.** (a) The bipath consists of two paths  $\Gamma_1$  and  $\Gamma_2$  that start and end at the point  $A$ . Both paths cross  $C$  at the point  $B$  and continue inside  $W$ .  $\Gamma_1$  lies on  $W_+$  while  $\Gamma_2$  lies on  $W_-$ . Finally, both paths end at  $A$ . (b) Depiction of the bipath in the unfolded bifurcation diagram.

$g_0(B^-)$  the limits of the homology cycles as we approach  $B \in C$  on  $W^+$  and  $W^-$ , respectively. But recall from (11) that  $g_0(B) = g_0(B^-) + g_0(B^+)$ .

Then we parallel transport  $g_0(B^+)$  along  $\Gamma_1$  back to  $A$  where it is mapped to  $g_0(A)$ . This can be deduced from the definition of  $g_0$ . We do the same with  $g_0(B^-)$  which we parallel transport along  $\Gamma_2$  back to  $A$ ; this cycle is also mapped to  $g_0(A)$ .

The two  $b(A)$  cycles evolve in a simpler way. When we cross  $C$  each one of the cycles goes to a distinct fiber. So one cycle  $b(B)$  goes to  $b(B^+)$  and the other one goes to  $b(B^-)$ . Since the cycle  $b$  is globally defined in a smooth way, when these cycles are parallel transported back to  $A$  along  $\Gamma_1$  and  $\Gamma_2$ , respectively, they are mapped to  $b(A)$ .

Therefore, we started with homology cycles  $\{2b(A), g_0(A)\}$  on the fiber  $\mathbf{T}_A^2$  and we ended with two copies of the same fiber  $\mathbf{T}_A^2$  with the same homology cycles  $\{b(A), g_0(A)\}$  on both of them. The final step is to *merge* the two bases by adding cycles together to obtain the cycles  $\{2b(A), 2g_0(A)\}$ . Thus the parallel transport of homology cycles along the bipath in the way described above gives the *bidromy* transformation

$$\{2b(A), g_0(A)\} \mapsto \{2b(A), 2g_0(A)\}. \tag{12}$$

The matrix that connects the two sets of homology cycles is

$$\begin{pmatrix} 1 & 0 \\ 0 & 2 \end{pmatrix}.$$

**Remark 2.** If we consider the initial basis  $\{2b(A), g_k(A) = g_0(A) + kb(A)\}$ ,  $k \in \mathbf{Z}$ , then by applying transformation (12) we obtain that

$$\{2b(A), g_k(A)\} \mapsto \{2b(A), 2g_k(A) - kb(A)\},$$

which is given by the matrix

$$\begin{pmatrix} 1 & 0 \\ -\frac{k}{2} & 2 \end{pmatrix}.$$

Note that this matrix has a fractional entry  $-k/2$  for  $k$  odd. This is reminiscent of fractional monodromy. The essential difference between fractional monodromy and bidromy is that in the former case, the fractional entry cannot be removed by any change of basis<sup>5</sup>. Thus it is

<sup>5</sup> They can however be removed by taking a suitable covering space [27].

a characteristic property of fractional monodromy and it arises because of the ‘twist’ of the curled tori [13]. On the other hand, in bidromy, it is possible to eliminate any non-diagonal matrix entry by a change of basis.

**Remark 3.** When we cross  $\mathcal{C}$  the cycle  $g_k(B) = g_0(B) + kb(B)$  can break into two parts in several possible ways as  $g_0(B^+) + k_+b(B^+)$  and  $g_0(B^-) + k_-b(B^-)$  with  $k_+ + k_- = k$ . This is also true for  $g_0(B)$  which can break into  $g_0(B^+) + k_+b(B^+)$  and  $g_0(B^-) - k_+b(B^-)$ . Parallel transport of any such choice back to  $A$  and merging of the resulting cycles gives the same result  $2g_0(A) + kb(A)$ . This means that the operation of parallel transport along the bipath is well defined. Note that only after considering *both* paths of the bipath, and merging the cycles at  $A$ , the final result does not depend on the choice of splitting at  $B$ .

### 2.5. Construction of homology basis and the rotation number

Consider a point  $\bar{f} \in \bar{\mathbf{R}}$  and denote by  $\mathbf{T}^2(\bar{f})$  the smooth two-dimensional fiber of  $F$  over  $\bar{f}$ . We want to use the flows of  $X_J$  and  $X_H$  in order to construct the representatives of two homology cycles that will constitute a basis of the first homology group  $H_1(\mathbf{T}^2(\bar{f}), \mathbf{Z}) \simeq \mathbf{Z}^2$ . Such cycle representatives can be generated by the flow of the vector fields that correspond to action variables.

A second vector field  $X_S$  on  $\mathbf{T}^2(\bar{f})$  that has a  $2\pi$  period is constructed in the following standard way, see [28]. Consider a point  $p \in \mathbf{T}^2(\bar{f})$  and the closed orbit  $\gamma_1(\bar{f})$  of the vector field  $X_J$  that starts at  $p$ . The *first return time*  $T(\bar{f})$  is the time that it takes for an orbit of the Hamiltonian vector field  $X_H$  that starts at  $p$  to cross again  $\gamma_1(\bar{f})$  at a point  $p'$ . A *rotation number*  $\Theta(\bar{f})$  is any  $t \in \mathbf{R}$  such that  $p$  goes to  $p'$  after time  $t$  along an orbit of  $X_J$ . Thus  $\Theta$  is defined only up to an arbitrary integer multiple of  $2\pi$ . The functions  $\Theta$  and  $T$  are constant on  $\mathbf{T}^2(\bar{f})$ , i.e. they do not depend on the choice of the initial point  $p$ , and they are locally smooth functions of  $\bar{f}$ . Furthermore,  $T(\bar{f})$  is a globally smooth univalued function in  $\bar{\mathbf{R}}$ . The required vector field of the second action can be defined as

$$X_S = -\frac{\Theta(\bar{f})}{2\pi} X_J + \frac{T(\bar{f})}{2\pi} X_H. \tag{13}$$

Note that if  $S$  is the action defined implicitly by the vector field  $X_S$  then  $S + kJ$ ,  $k \in \mathbf{Z}$  is also an action. This freedom in the choice of the action corresponds to the freedom in the choice of the rotation number  $\Theta$ . Furthermore note that  $X_S = \pm X_{I_0} + k_S X_J$ ,  $k_S \in \mathbf{Z}$ , where  $I_0$  is the good action in  $\bar{\mathbf{R}}$  constructed in section 2.3.

## 3. Two examples

In this section, we consider two examples of integrable Hamiltonian systems with a swallowtail. The description of the swallowtail from the classical point of view has been completed in section 2. Here, we focus on the quantum spectrum and, in particular, the parallel transport of quantum cells along a bipath and their continuation through the curve  $\mathcal{C}$  of the bitoric.

### 3.1. A simple Hamiltonian swallowtail

We consider a Hamiltonian system on  $\mathbf{R}^2 \times \mathbf{S}^1 \times \mathbf{R}$  with coordinates  $(q, p, \phi, J)$  and the symplectic form  $\omega = dq \wedge dp + d\phi \wedge dJ$ . The Hamiltonian function is

$$H = \frac{1}{2}p^2 + \frac{1}{4}q^4 - \frac{1}{2}q^2 + Jq. \tag{14}$$

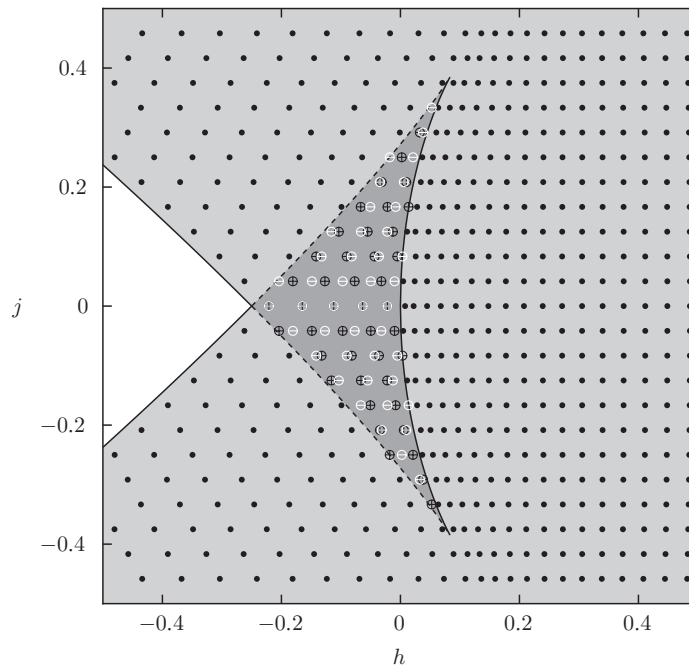


**Figure 6.** The bifurcation diagram  $\mathcal{BD}$  of  $F$  for the canonical swallowtail system and the joint quantum spectrum. The light gray area represents regular values  $(h, j)$  such that  $F^{-1}(f)$  consists only of one component while the dark gray area represents the two-component region  $W$ . Points of the quantum spectrum outside  $W$  are represented by black dots. Points on  $W_+$  are represented by a black circle with a + sign inside and points on  $W_-$  are represented by a white circle with a - sign inside. The value of  $\hbar$  is  $1/24$ .

Since  $J$  is an integral of motion for  $H$ , the system is *Liouville integrable* with integral map  $F = (H, J)$ . By construction,  $J$  is a global action. A part of the  $\mathcal{BD}$  of  $F$  is depicted in figure 7 together with the joint quantum spectrum of the system.

The flow of  $X_J$  defines an  $\mathbf{S}^1$  action on  $\mathbf{R}^2 \times \mathbf{S}^1 \times \mathbf{R}$  given by

$$t, (q, p, \phi, J) \mapsto \phi^t(q, p, \phi, J) = (q, p, \phi + t, J).$$

The algebra of  $\mathbf{S}^1$ -invariant polynomials is freely generated by  $(q, p, J)$ ; therefore, for fixed  $J = j$  the reduced space is  $\mathbf{R}^2$  with coordinates  $(q, p)$ . The reduced Hamiltonian is

$$H_j = \frac{1}{2}p^2 + \frac{1}{4}q^4 - \frac{1}{2}q^2 + jq. \tag{15}$$

Thus we obtain a 1-DOF Hamiltonian system on  $\mathbf{R}^2$  with potential  $V_j(q) = \frac{1}{4}q^4 - \frac{1}{2}q^2 + jq$  that describes precisely the swallowtail catastrophe [29], see figure 6. By construction,  $F^{-1}(h, j) = H_j^{-1}(h) \times \mathbf{S}^1$ . Furthermore, note that the two-dimensional surface  $\{\phi = 0, J = j\}$  is a Poincaré surface  $\Sigma_j$  in  $J^{-1}(j) \simeq \mathbf{R}^2 \times \mathbf{S}^1$  which can be described by the coordinates  $(q, p)$ . Thus,  $H_j = H|_{\Sigma_j}$ . This means that the representatives  $\gamma(\bar{f})$  of the homology cycles  $g(\bar{f})$  for  $\pi(\bar{f}) = (h, j)$ , as defined in section 2.1, are the connected components of the level sets  $H_j^{-1}(h)$ . In figure 8, we show level sets  $H_j^{-1}(h)$  for  $j = 1/10$ , cf figure 4.

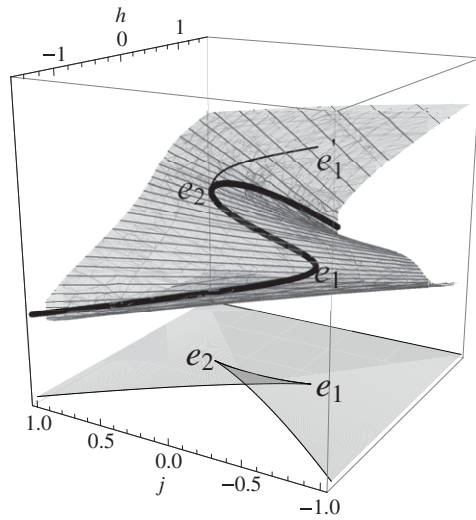


**Figure 7.** Following [29] we depict in the space  $(h, j, q)$  the surface  $Z$  defined by  $V_j(q) = h$ , where  $V_j(q) = q^4/4 - q^2/2 + jq$  is the reduced potential in (15). The surface  $Z$  is projected to the  $(h, j)$  plane where the discriminant locus of the equation  $V_j(q) = h$  is also depicted. This discriminant locus is precisely the set of critical values of the integral map  $F = (H, J)$  and geometrically it corresponds to values of  $(h, j)$  for which the vertical line  $\{(h, j, s), s \in \mathbf{R}\}$  is tangent to  $Z$  at a point  $q_0(h, j)$ . The set  $(h, j, q_0(j, h))$  for  $(h, j)$  in the discriminant locus is depicted by the thick black curve  $Z_0$  on the surface  $Z$ . The curve  $Z_0$  separates  $Z$  into two parts. Either one of these parts (together with  $Z_0$ ) can represent the unfolded bifurcation diagram  $\overline{BD}$  of the system (14) if certain points are identified. In particular, we can recover the  $\overline{BD}$  if we consider the upper part of  $Z$  together with  $Z_0$  and then glue the piece  $e_1e_2$  of the curve  $Z_0$  with the curve  $e'_1e_2$ , cf figure 1(b). Both of these two pieces project vertically to the part of the discriminant locus between the points  $e_1$  and  $e_2$ .

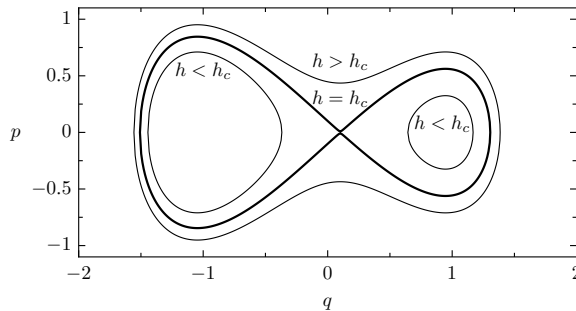


**Figure 8.** Level sets  $H_j^{-1}(h)$  for  $j = 0.1$  and different values of  $h$ . In the figure,  $h_c \approx 0.005067$  is the value of the energy for which  $(h_c, j) \in \mathcal{C}$ . The corresponding level set  $H_j^{-1}(h_c)$  is represented by the thick figure-8 curve. For  $h = -0.1 < h_c$  the level curve  $H_j^{-1}(h)$  consists of two connected components, while for  $h = 0.1 > h_c$  the corresponding level curve has a single component.

The value  $I_0(\bar{f})$  of the good action on a fiber  $\mathbf{T}^2(\bar{f})$  that has an intersection  $\gamma(\bar{f})$  with  $\Sigma_j$  is

$$I_0(\bar{f}) = \frac{1}{2\pi} \oint_{\gamma(\bar{f})} p dq.$$

Contour lines of  $I_0$  for values given by  $(k + 1/2)\hbar$  are shown in figure 9.

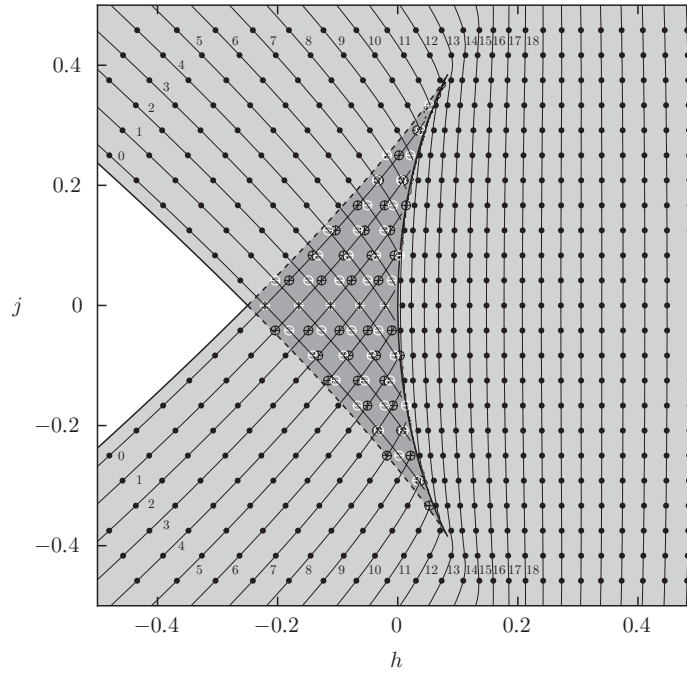


**Figure 9.** Contours of the good action  $I_0$  in the simple swallowtail system. The values of  $I_0$  are  $(k + 1/2)\hbar$  where  $\hbar = 1/24$ . We depict the value of  $k$  for several contours.

In section 2.4, we described in detail the parallel transport of homology cycles along a bipath. Here we describe the parallel transport of quantum cells in the joint quantum spectrum of the system. For a review of the relation between the basis of the first homology group and quantum cells see appendix A.

In figure 10(a), we show the parallel transport of a quantum cell along a bipath. The initial cell  $Q(A)$  (white filled in figure 10(a)) is spanned by the vectors  $\{2\vec{b}(A), \vec{g}(A)\}$ . The vectors  $\vec{b}(A)$  and  $\vec{g}(A)$  are defined by the relations

$$\begin{aligned} \vec{g}(A) \cdot \nabla J(A) &= \vec{b}(A) \cdot \nabla I(A) = \hbar, \\ \vec{g}(A) \cdot \nabla I(A) &= \vec{b}(A) \cdot \nabla J(A) = 0, \end{aligned}$$

and they correspond to the homology cycles  $b(A)$  and  $g(A)$ , respectively.

First, the cell  $Q(A)$  is parallel transported toward the point  $B$  at  $C$ . As the bipath crosses  $C$  and enters  $W$ , the cell splits into two parts and at an interior point  $C$  of  $W$  we have the cell  $Q(C^+)$  on  $W_+$  and the cell  $Q(C^-)$  on  $W_-$ , see figure 10(b).

The continuation of the quantum cell through  $C$  is carried out in the following way. For the given initial quantum cell  $Q(A)$  at the point  $A$  outside  $W$  (the initial white cell in our figures), we find the corresponding homology cycles  $b(A)$  and  $g(A)$ . Then we continue the homology cycle  $g(A)$  through  $C$  up to points  $C^+ \in W_+$  and  $C^- \in W_-$  that belong in the joint quantum spectrum and we obtain two homology cycles  $g(C^+)$  and  $g(C^-)$ . Then we can identify the actions  $I_+$  and  $I_-$  on  $W_+$  and  $W_-$ , respectively, that generate  $g(C^+)$  and  $g(C^-)$ . At the final step, we define the corresponding quantum cells  $Q(C^\pm)$  using the relations

$$\begin{aligned} \vec{g}(C^\pm) \cdot \nabla J(C^\pm) &= \vec{b}(C^\pm) \cdot \nabla I_\pm(C^\pm) = \hbar, \\ \vec{g}(C^\pm) \cdot \nabla I_\pm(C^\pm) &= \vec{b}(C^\pm) \cdot \nabla J(C^\pm) = 0, \end{aligned}$$

see appendix A. Using this approach we obtained the splitting of cells shown in figure 10.

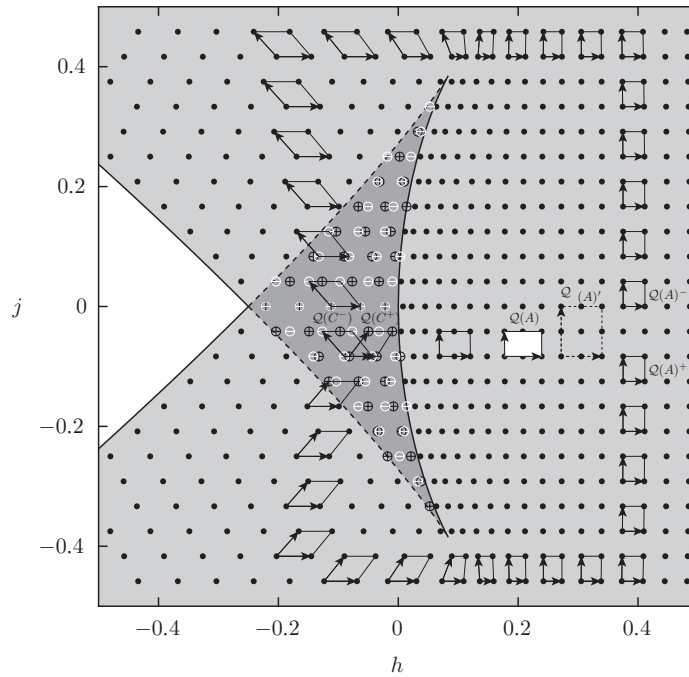


Figure 10. Parallel transport along a bipath and continuation of cells through  $\mathcal{C}$ .

**Remark 4.** The continuation of the initial cell through  $\mathcal{C}$  and the subsequent splitting are not obvious when working solely with the joint spectrum. There are several reasons for this difficulty. First, the joint spectrum gives a coarse grained picture of the geometry near  $\mathcal{C}$  since it misses structures smaller than  $\hbar$ . Furthermore, this picture is distorted by the existence of tunneling effects near the potential barrier at  $\mathcal{C}$ . Such problems do not appear in the classical description where we can distinguish fine details of the geometry. Thus we continue quantum cells through  $\mathcal{C}$  by using our detailed knowledge of the geometry of the classical system near  $\mathcal{C}$ .

After crossing  $\mathcal{C}$  we continue the parallel transport of the cells  $Q(C^\pm)$  along the two parts of the bipath back to  $A$ . Thus we obtain two cells that we denote by  $Q(A)^\pm$ . Each of these, is spanned by the vectors  $\{\vec{b}(A), \vec{g}(A)\}$ . Finally, at  $A$  we merge these two cells by adding together the vectors that span them. The result is the cell  $Q(A)'$  spanned by the vectors  $\{2\vec{b}(A), 2\vec{g}(A)\}$ . Thus the transformation in terms of cell-spanning vectors is

$$\{2\vec{b}(A), \vec{g}(A)\} \mapsto \{2\vec{b}(A), 2\vec{g}(A)\},$$

which is essentially identical to (12).

**Remark 5.** The homology basis  $\{b(A), g_k(A)\}$  with  $g_k(A) = g(A) + kb(A)$ ,  $k \in \mathbf{Z}$  corresponds to the quantum cell spanned by the vectors  $\{\vec{b}(A), \vec{g}_k(A)\}$  where  $\vec{g}_k(A) = \vec{g}(A) - k\vec{b}(A)$ . The transformation of the latter along the bipath is

$$\{2\vec{b}(A), \vec{g}_k(A)\} \mapsto \{2\vec{b}(A), 2\vec{g}_k(A) + k\vec{b}(A)\},$$

cf remark 2.

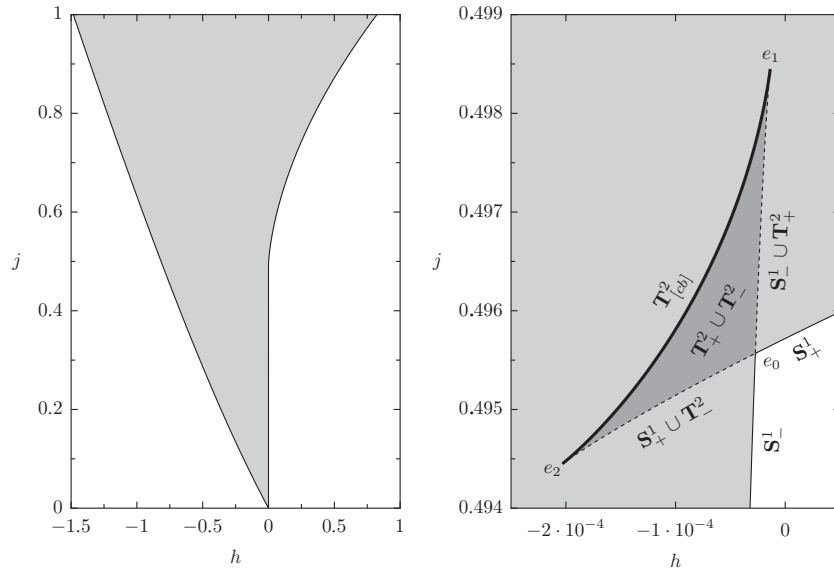


**Figure 11.** Bifurcation diagram  $\mathcal{BD}$  for the integral map  $F$  (18) and for  $\ell = 3 \cdot 10^{-4}$  and  $y = 10^{-1}$ . The  $\mathcal{BD}$  for a wide range of  $(h, j)$  values is shown on the right and a detail on the left. Points in the light gray region lift to smooth tori  $\mathbf{T}^2$ . Points in the dark gray region lift to the disjoint union of two tori  $\mathbf{T}^2$ . Points along the dashed curves lift to the disjoint union  $\mathbf{S}^1 \cup \mathbf{T}^2$ . Points along the thick curve lift to the bitori  $\text{bi}\mathbf{T}^2$ .

### 3.2. The reduced 1:1:2 resonant system

In this section, we analyze a 2-DOF Hamiltonian system in  $\mathbf{R}^4$  obtained by reduction of one of the symmetries of the 3-DOF Hamiltonian system studied in [14]. The reduction procedure is described in detail in appendix B. The Hamiltonian function is

$$H = (P_1 P_2 + Q_1 Q_2)(2\ell + P_2^2 + Q_2^2)^{1/2} - (\ell + P_2^2 + Q_2^2) + \frac{1}{2}(1 + y)(\ell + P_2^2 + Q_2^2)^2, \quad (16)$$

where  $\ell > 0$  and  $y$  are real parameters. The Hamiltonian function (16) commutes with

$$J = \frac{1}{2}(Q_1^2 + Q_2^2 + P_1^2 + P_2^2). \quad (17)$$

Thus  $H$  and  $J$  define a Liouville integrable Hamiltonian system with integral map  $F$  given by

$$F(Q, P) = (H(Q, P), J(Q, P)). \quad (18)$$

For the computation of the bifurcation diagram  $\mathcal{BD}$  of  $F$  (18), we used standard methods described in [20, 28]. The result of the numerical computation is depicted in figure 11.

The most straightforward way to compute the good action  $I_0$  for this example is to reduce the  $\mathbf{S}^1$  action generated by the flow of  $X_J$  (which represents a 1:1 resonant oscillator) on  $\mathbf{R}^4$ . The reduction of the 1:1 resonance is well known [28]. The reduced system is a 1-DOF Hamiltonian system on the reduced space

$$P_j = \{(\sigma_1, \sigma_2, \sigma_3) \in \mathbf{R}^3 : \sigma_1^2 + \sigma_2^2 + \sigma_3^2 = j^2\} \simeq \mathbf{S}_j^2,$$

where  $\sigma_1 = Q_1 Q_2 + P_1 P_2$ ,  $\sigma_2 = Q_2 P_1 - Q_1 P_2$ ,  $\sigma_3 = \frac{1}{2}(Q_1^2 + P_1^2 - Q_2^2 - P_2^2)$  and  $J = j$ . We introduce coordinates  $(z, \phi)$  on  $\mathbf{S}_j^2$  with  $\sigma_3 = z$  and  $(\sigma_1, \sigma_2) = \sqrt{j^2 - z^2}(\cos \phi, \sin \phi)$ . Then the reduced symplectic form  $\varpi_j$  on  $P_j$  can be written as

$$\varpi_j = \frac{1}{2} d\phi \wedge dz.$$

A fiber  $\mathbf{T}^2(\bar{f})$  of the system is mapped to the reduced space  $P_j$  to a closed curve  $\gamma(\bar{f})$ . Then the good action  $I_0$  is given by

$$I_0(\bar{f}) = \frac{1}{2\pi} \oint_{\gamma(\bar{f})} \frac{1}{2} z d\phi. \tag{19}$$

The contour lines of the good action are depicted in figure 12.

In figure 13, we show the joint spectrum for the integral map  $F$  and the parallel transport of two different double quantum cells along a bipath. For the parallel transport and the continuation through the bitorus line  $C$  of the quantum cells, we use the same methods and ideas described analytically in section 3.1.

In figure 13(a) we have chosen the same initial double quantum cell  $Q(A)$  as in the parallel transport shown in figure 18 of [14]. The cell  $Q(A)$  is spanned by the vectors  $\{2\vec{b}(A), \vec{g}'(A)\}$ . Just as in [14] we obtain after the parallel transport along the bipath the two quantum cells  $Q(A)^+$  and  $Q(A)^-$  spanned by the vectors  $\{\vec{b}(A), \vec{g}'(A)\}$  and  $\{\vec{b}(A), \vec{g}'(A)+\vec{b}(A)\}$ , respectively. Finally we merge the two cells to obtain the final cell  $Q(A)'$  spanned by  $\{2\vec{b}(A), 2\vec{g}'(A)+\vec{b}(A)\}$ . This transformation of the initial cell  $Q(A)$  to the final cell  $Q(A)'$  was observed in [14].

The parallel transport of a different choice of initial double cell  $Q(A)$  is shown in figure 13(b). In this case,  $Q(A)$  is spanned by the vectors  $\{2\vec{b}(A), \vec{g}(A)\}$  where  $\vec{b}(A)$  and  $\vec{g}(A)$  are the vectors that we obtain from considering the actions  $J$  and  $I$  with the latter being the unique good action in this system. The final result is the cell  $Q(A)'$  spanned by the vectors  $\{2\vec{b}(A), 2\vec{g}(A)\}$ .

**Remark 6.** Note that our merging of the cells  $Q(A)^+$  and  $Q(A)^-$  differs from the merging in [14]. In [14] the cells are merged by using the fact that one of their sides is spanned by the same vector  $\vec{b}(A)$ . The side of the merged cell is also taken to be  $\vec{b}(A)$  and the vectors for the second side  $\vec{g}'(A)$  and  $\vec{g}'(A) + \vec{b}(A)$  are added together. Thus in [14] the obtained transformation is

$$\{2\vec{b}(A), \vec{g}'(A)\} \mapsto \{\vec{b}(A), 2\vec{g}'(A) + \vec{b}(A)\},$$

given by the matrix<sup>6</sup>

$$\begin{pmatrix} \frac{1}{2} & 0 \\ \frac{1}{2} & 2 \end{pmatrix}.$$

We believe that the choice of merging in [14] is not correct. First, it cannot be generalized to the case where there is no globally defined action. In such case the two final cells that should be merged may not have a common side since  $\vec{v}_1(A)$  itself may change after parallel transport along the bipath. Second, it does not agree with the corresponding natural merging of homology cycles defined in section 2.4.

### 3.3. Comparison of the two examples

We have seen that the two systems studied in sections 3.1 and 3.2 have the same qualitative characteristics: they both have the same fibration (near the swallowtail), a unique good action and the parallel transport of homology cycles or quantum cells gives exactly the same results for the two systems. So it is surprising that the concept of bidromy was introduced in the much more complicated example of the 3-DOF 1:1:2 resonant system. It is even more surprising that it was believed that systems like the simple swallowtail of section 3.1 do not have bidromy. So the natural question to be asked, is what distinguishes these two examples.

<sup>6</sup> The off-diagonal element in the matrix written in equation (18) of [14] for the above transformation appears as 1.

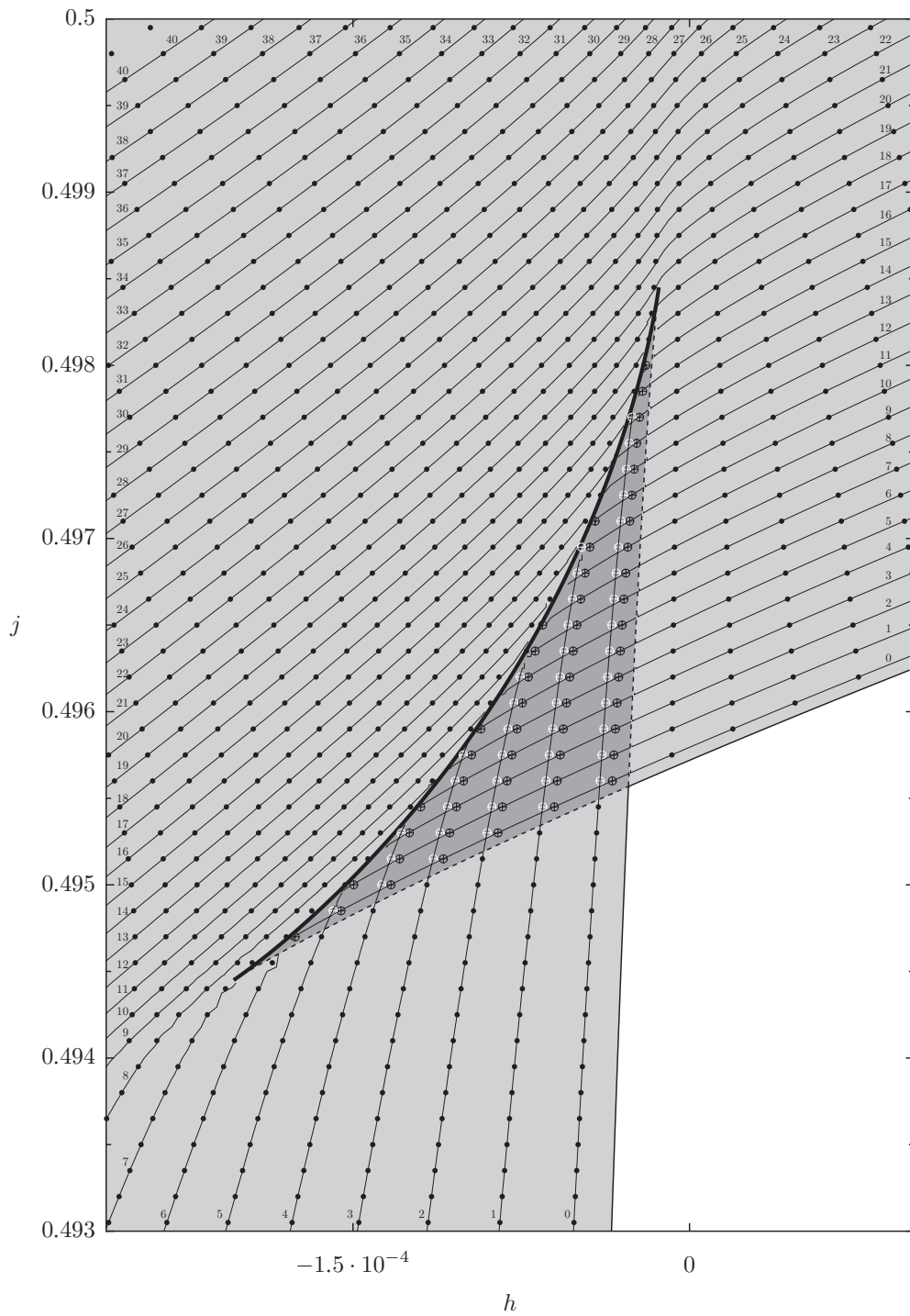


**Figure 12.** Contours of the good action  $I_0$  (19) for values  $\hbar(k + 1/2)$  with  $k = 0, 1, 2, \dots$ . The parameters used in the figure are  $y = 10^{-1}$ ,  $\hbar = 1.5 \times 10^{-4}$ ,  $\ell = 2\hbar$ . The contour lines are labeled by the integer  $k$ .

In figure 13, we note that the points of the spectrum that belong in  $W_+$  and  $W_-$  are arranged in almost parallel lines. This gives a very strong indication on how the initial (white) quantum cell  $\mathcal{Q}(A)$  in figure 13(a) can be continued through  $\mathcal{C}$  and how it should be broken into two cells. This is exactly what was done in [14]. On the other hand, it is not at all obvious how to continue the initial cell through  $\mathcal{C}$  in the simple swallowtail in figure 10. We have solved this problem by looking at the behavior of homology cycles and taking advantage of the correspondence between homology cycles and quantum cells.

The reason behind the observed differences in the joint spectra of the two systems is that there is a significant *quantitative* difference between the reduced 1:1:2 resonant system and the simple swallowtail. In particular, we have found numerically that the rotation number in the reduced 1:1:2 resonant system satisfies the relation

$$\Theta(\bar{f}^+) - \Theta(\bar{f}^-) = 0 \pmod{2\pi}, \tag{20}$$

where  $\pi(\bar{f}^+) = \pi(\bar{f}^-) = f$ , while in the simple swallowtail we have

$$\Theta(\bar{f}^+) - \Theta(\bar{f}^-) = 2\pi\sqrt{2} \pmod{2\pi}. \tag{21}$$

For both the reduced 1:1:2 resonant system and the simple swallowtail, we have that  $T(\bar{f}^+) = T(\bar{f}^-)$ .

Recall (see appendix A) that the quantum cell  $\mathcal{Q}(\bar{f})$  is spanned by the vectors  $\vec{b}(\bar{f}) = \hbar(0, \nu(\bar{f}))$  and  $\vec{g}(\bar{f}) = \hbar(1, \nu(\bar{f})\Theta(\bar{f}))$ , where  $\nu(\bar{f}) = 1/T(\bar{f})$ . Note that for both systems we have that  $\vec{b}(\bar{f}^+) = \vec{b}(\bar{f}^-)$ . Moreover, for the reduced 1:1:2 system, we can choose the branches of  $\Theta$  in such a way that  $\Theta(\bar{f}^+) = \Theta(\bar{f}^-)$  and consequently  $\vec{g}(\bar{f}^+) = \vec{g}(\bar{f}^-)$ . This fact gives the parallel arrangement of the spectrum points in  $W$  for the reduced 1:1:2 system. In the simple swallowtail system we have that

$$\vec{g}(\bar{f}^+) - \vec{g}(\bar{f}^-) = \hbar(0, 2\pi\nu(\bar{f})(k + \sqrt{2})), \quad k \in \mathbf{Z},$$

which does not vanish for any  $k$ .

**Remark 7.** We have verified the validity of equations (20) and (21) only numerically. A rigorous proof of these results based on the complex analytic methods introduced in [12] is given in a forthcoming paper.

#### 4. Discussion

Since [14], where bidromy was initially proposed, the 1:1:2 resonant system has been the only relevant example. In this paper, we expand considerably this class of examples by showing that all systems with a swallowtail structure are qualitatively the same. We have analyzed in detail the properties of global action coordinates in systems with swallowtails and we proved the existence of a unique good action. Furthermore, we have defined the continuation of homology cycles and quantum cells through the curve  $\mathcal{C}$  of critical values. Following [14] we defined the bidromy transformation along a bipath and we showed that as a result of the existence of a unique good action, there is a unique basis of the first homology group (or correspondingly a unique quantum cell) for which the bidromy transformation is diagonal.

More importantly, this paper demonstrates that the analysis of integrable Hamiltonian systems near a critical fiber is not sufficient to provide a complete understanding of the system. For the latter we need to study the global effect of families of critical fibers. Such families come in many different combinations and thus such a program can never be exhausted. Nevertheless, some particular cases such as systems with families of curled tori that give rise to fractional monodromy or systems with families of bitori like the swallowtail systems studied here are worth studying since they appear in physical applications.

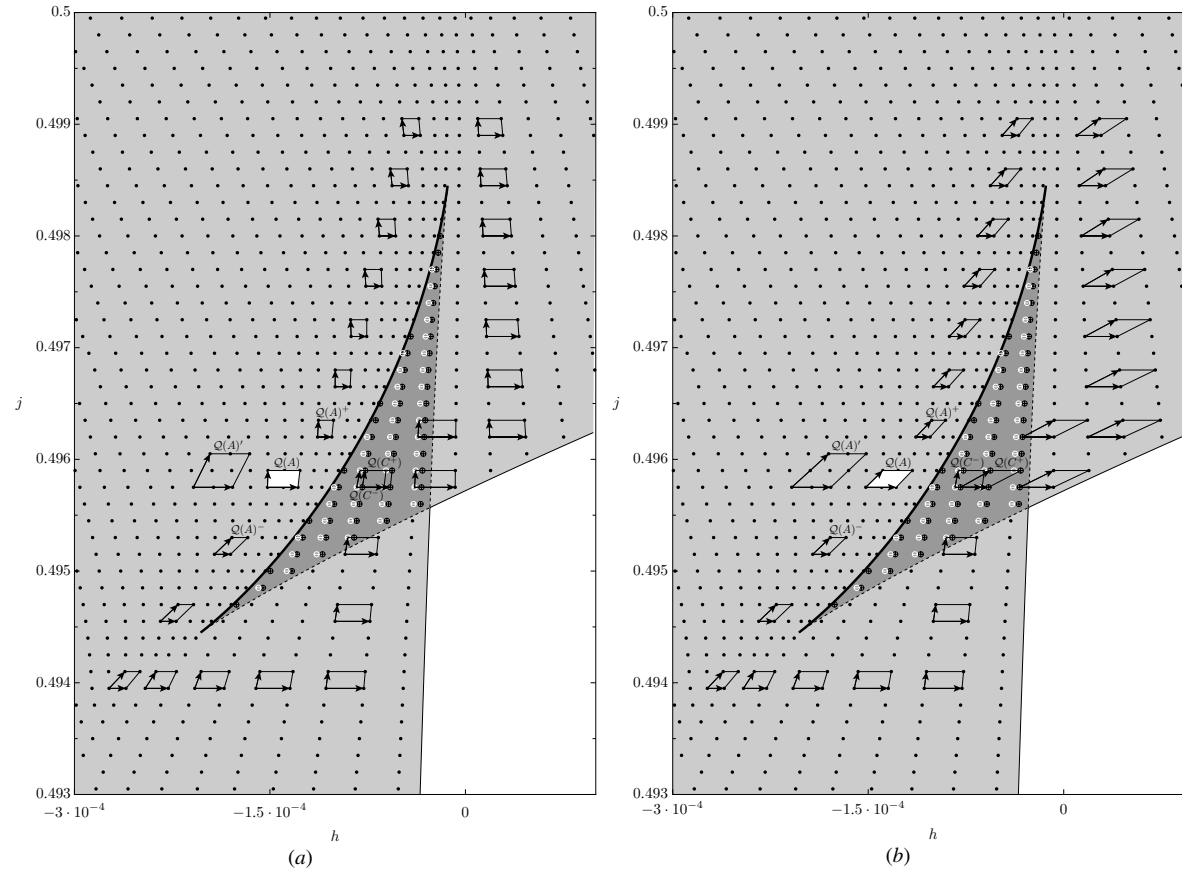


**Figure 13.** Quantum spectrum of the system with Hamiltonian  $H(16)$  and parallel transport of quantum cells along a bipath. The parameters used are  $y = 10^{-1}$ ,  $\hbar = 1.5 \times 10^{-4}$ ,  $\ell = 2\hbar$ .

More complicated examples can also be found in physical problems. For example in [30], it is shown that the hydrogen atom in 1:2 resonance has typically a combination of a swallowtail and two 1-parameter families of curled tori that are attached to the swallowtail, see also [24]. Another example is provided by the HOCl molecule [31]. In this system a 1-parameter family of curled tori intersects a 1-parameter family of bitori giving rise to a more complicated geometry and an intricate structure of the quantum spectrum. Such arrangements of singular fibers can only be understood if we examine the whole set of singular fibers and the way they are embedded in the Lagrangian fibration. The ultimate reward of this research program will be the ability to describe completely the fibration of the phase space and the structure of the joint spectrum in systems with very complicated arrangements of lines of bitori, curled tori, pinched tori, etc in a simple way—ideally, by decomposing such systems to simpler ‘building blocks’ from which we will then be able to reconstruct the complete geometry of the fibration.

### Acknowledgments

The authors would like to thank Hans Jauslin, Pavao Mardešić, Michele Pelletier, Dmitrii Sadoivskiĭ and Boris Zhilinskiĭ, for useful discussions. KE also thank the Université du Littoral, Dunkerque and the Institut Carnot de Bourgogne, Dijon, where part of this research was carried out, for their hospitality. KE was supported by the NWO cluster NDNS<sup>+</sup>.

### Appendix A. Relation between rotation numbers, homology cycles and quantum cells

In order to relate the continuation of homology basis in previous sections to the parallel transport of quantum elementary cells we give here the basic ideas of the correspondence.

Consider a  $K$ -DOF Liouville integrable Hamiltonian system in  $\mathbf{R}^{2K}$  with integral map  $F = (F_1, \dots, F_K)$  and a neighborhood of  $\mathbf{R}^{2K}$  where smooth actions  $(I_1, \dots, I_K)$  can be defined. According to the semiclassical EBK approximation quantum states correspond to values of the actions of the form  $I_k = \hbar(n_k + \mu_k)$  for  $k = 1, \dots, K$  where  $n_k \in \mathbf{Z}$  and  $\mu_k$  is a constant correction term related to the Maslov index. Thus, in the action space, quantum states form a regular lattice. Mapping this lattice back to the integral space with coordinates  $(F_1, \dots, F_K)$ , we obtain a deformed lattice. Consider two adjacent points of the joint spectrum along a line of constant action  $I$ . The line segment that connects these points approximates the tangent to the curve  $I = \text{const}$  and the approximation becomes better as  $\hbar \rightarrow 0$ . Denote by  $\langle n_1, \dots, n_K \rangle_F$  the point  $P$  in the integral space such that  $I_k(P) = \hbar(n_k + \mu_k)$ ,  $k = 1, \dots, K$ . Then define by  $\vec{v}_k$  the vector from  $\langle n_1, \dots, n_k, \dots, n_K \rangle_F$  to  $\langle n_1, \dots, n_k + 1, \dots, n_K \rangle_F$ . The vector  $\vec{v}_k$  is tangent (in the limit  $\hbar \rightarrow 0$ ) to all the surfaces  $I_{k'} = \text{const}$  for  $k' \neq k$  and thus orthogonal to the gradient vectors

$$\nabla I_{k'} = \left( \frac{\partial I_{k'}}{\partial F_1}, \dots, \frac{\partial I_{k'}}{\partial F_K} \right).$$

Moreover,

$$\vec{v}_k \cdot \nabla I_{k'} = \hbar \delta_{kk'}. \tag{A.1}$$

Consider now in the same neighborhood two sets of actions  $I = (I_1, \dots, I_K)$  and  $I' = (I'_1, \dots, I'_K)$  that are related by

$$\begin{pmatrix} \nabla I'_1 \\ \vdots \\ \nabla I'_K \end{pmatrix} = A \begin{pmatrix} \nabla I_1 \\ \vdots \\ \nabla I_K \end{pmatrix}, \tag{A.2}$$

where  $A \in \text{GL}(K, \mathbf{Z})$ . Then the vectors  $\vec{v}'_k$  defined by  $\vec{v}'_k \nabla I'_{k'} = \hbar \delta_{kk'}$  are connected to  $\vec{v}_k$  through the relation

$$\begin{pmatrix} \vec{v}'_1 \\ \vdots \\ \vec{v}'_K \end{pmatrix} = (A^{-1})^t \begin{pmatrix} \vec{v}_1 \\ \vdots \\ \vec{v}_K \end{pmatrix}. \tag{A.3}$$

Also if we denote by  $X_H$  the Hamiltonian vector field that corresponds to the function  $H$ , we have that

$$X_{I_{k'}} = \sum_{k=1}^K \frac{\partial I_{k'}}{\partial F_k} X_{F_k}, \tag{A.4}$$

i.e. in the basis  $(X_{F_1}, \dots, X_{F_K})$ , the vector field  $X_{I_{k'}}$  has the same components as the gradient vector field  $\nabla I_{k'}$ . This implies that the vector fields  $X_{I'_{k'}}$  are related to  $X_{I_k}$  by

$$\begin{pmatrix} X_{I'_1} \\ \vdots \\ X_{I'_K} \end{pmatrix} = A \begin{pmatrix} X_{I_1} \\ \vdots \\ X_{I_K} \end{pmatrix}. \tag{A.5}$$

Finally, the homology cycles  $g_k$  and  $g'_k$  generated by the flows of the vector fields  $X_{I_k}$  and  $X_{I'_k}$  respectively are related through

$$\begin{pmatrix} g'_1 \\ \vdots \\ g'_K \end{pmatrix} = A \begin{pmatrix} g_1 \\ \vdots \\ g_K \end{pmatrix}. \tag{A.6}$$

In the specific case of a 2-DOF integrable system with the integral map  $F = (F_1, F_2)$  where  $F_2 = H$  is the Hamiltonian function and  $F_1 = I_1 = J$  is a globally defined action, the vector field  $X_{I_2}$  is given by

$$X_{I_2} = -\Theta X_{F_1} + T X_{F_2}. \tag{A.7}$$

Thus,  $\nabla I_2 = (-\Theta, T)$  while  $\nabla I_1 = (1, 0)$ . Using (A.1) we obtain that  $\vec{v}_2 = \hbar(0, 1/T)$  and  $\vec{v}_1 = \hbar(1, \Theta/T)$ . Note that  $\vec{v}_2$  has a constant direction and only its length changes but since the first return time  $T$  is a globally smooth function and  $T \neq 0$ ,  $\vec{v}_2$  defines globally a smooth vector field. On the other hand the slope of  $\vec{v}_1$  is determined by the ratio  $\Theta/T$  and since  $\Theta$  is in general a multivalued function so is  $\vec{v}_1$ .

Furthermore, note that in 2-DOF systems if we have two homology bases  $\{g_1, g_2\}$  and  $\{g'_1, g'_2\}$  that are related through a matrix  $M \in \text{SL}(2, \mathbf{Z})$ , then the corresponding vectors  $\{\vec{v}_1, \vec{v}_2\}$  and  $\{\vec{v}'_1, \vec{v}'_2\}$  are related through  $(M^{-1})^t$  but if we denote  $\vec{g}_1 = \vec{v}_2$  and  $\vec{g}_2 = -\vec{v}_1$  then we obtain that  $(\vec{g}'_1, \vec{g}'_2)^t = M \cdot (\vec{g}_1, \vec{g}_2)^t$ . Thus we associate the homology cycle  $g_k, k = 1, 2$ , to the vector  $\vec{g}_k$ . Note that this association does not have an analog in more dimensions.

### Appendix B. Reduction of the 1:1:2 resonant system to 2-DOF

The 3-DOF Hamiltonian studied in [14] is

$$H = S - R + \frac{1}{2}(1 + y)R^2, \tag{B.1}$$

where  $y$  is a real parameter. The functions  $S, R$  are invariants of the  $\mathbf{T}^2$  group action generated by the flows of the vector fields  $X_N, X_L$  of, respectively, the 1:1:2 resonance

$$N = \frac{1}{2}(2p_1^2 + p_2^2 + p_3^2 + 2q_1^2 + q_2^2 + q_3^2),$$

and the angular momentum

$$L = p_3q_2 - p_2q_3.$$

In particular,

$$\begin{aligned} S &= \frac{1}{2}(2p_1(p_2q_2 + p_3q_3) + q_1(q_2^2 + q_3^2 - p_2^2 - p_3^2)), \\ R &= \frac{1}{2}(p_2^2 + p_3^2 + q_2^2 + q_3^2). \end{aligned}$$

There is one more invariant

$$T = \frac{1}{2}(2q_1(p_2q_2 + p_3q_3) - p_1(q_2^2 + q_3^2 - p_2^2 - p_3^2))$$

that does not appear in the following. In this section we reduce the Hamiltonian (B.1) to 2-DOF by reducing the  $\mathbf{S}^1$  group action generated by the flow of  $X_L$ .

### B.1. Reduction to two degrees of freedom

The invariants of the flow of the Hamiltonian vector field  $X_L$  are  $q_1$ ,  $p_1$  and

$$\begin{aligned} \tau_1 &= \frac{1}{2}(p_2^2 + p_3^2 + q_2^2 + q_3^2), \\ \tau_2 &= \frac{1}{2}(-p_2^2 - p_3^2 + q_2^2 + q_3^2), \\ \tau_3 &= p_2q_2 + p_3q_3, \\ L &= p_3q_2 - p_2q_3. \end{aligned}$$

The Hamiltonian  $H$  (B.1) becomes after fixing  $L = \ell$

$$H = \frac{1+y}{2}(\ell^2 + \tau_2^2 + \tau_3^2) - \tau_1 + q_1\tau_2 + p_1\tau_3. \quad (\text{B.2})$$

Also

$$R = \tau_1,$$

and

$$N = p_1^2 + q_1^2 + \tau_1.$$

The syzygy is

$$\ell^2 = \tau_1^2 - \tau_2^2 - \tau_3^2. \quad (\text{B.3})$$

The Hamiltonian (B.2) after substituting  $\ell^2$  from (B.3) simplifies to

$$H = -\tau_1 + \frac{1+y}{2}\tau_1^2 + q_1\tau_2 + p_1\tau_3. \quad (\text{B.4})$$

The Poisson brackets between the invariants are

$$\begin{aligned} \{\tau_1, \tau_2\} &= -2\tau_3, \\ \{\tau_2, \tau_3\} &= 2\tau_1, \\ \{\tau_3, \tau_1\} &= -2\tau_2. \end{aligned}$$

### B.2. Canonical coordinates

The reduced space for  $\ell \neq 0$  is diffeomorphic to  $\mathbf{R}^4$  since it is the graph of the smooth function  $(q_1, p_1, \tau_2, \tau_3) \mapsto \tau_1 = (\ell^2 + \tau_2^2 + \tau_3^2)^{1/2}$ . Actually  $(q_1, p_1, \tau_2, \tau_3)$  is a global chart for this manifold but  $(\tau_2, \tau_3)$  are not canonically conjugate. We introduce canonical coordinates  $(Q_1, Q_2, P_1, P_2)$  using the following map which is a diffeomorphism for  $\ell > 0$ :

$$\begin{aligned} Q_1 &= q_1, \\ P_1 &= p_1, \\ Q_2 &= \tau_2 f^{1/2}, \\ P_2 &= \tau_3 f^{1/2}, \end{aligned}$$

where

$$f = \frac{(\tau_2^2 + \tau_3^2 + \ell^2)^{1/2} - \ell}{\tau_2^2 + \tau_3^2}.$$

Then

$$\{Q_2, P_2\} = 1.$$

The inverse of the above transformation is

$$q_1 = Q_1, \quad p_1 = P_1, \quad \tau_2 = Q_2 g^{1/2}, \quad \tau_3 = P_2 g^{1/2},$$

where

$$g = Q_2^2 + P_2^2 + 2\ell.$$

In the canonical coordinates  $(Q_1, P_1, Q_2, P_2)$ , we have

$$\tau_1 = \ell + P_2^2 + Q_2^2.$$

The Hamiltonian  $H$  (B.4) becomes

$$H = (P_1 P_2 + Q_1 Q_2)(2\ell + P_2^2 + Q_2^2)^{1/2} - (\ell + P_2^2 + Q_2^2) + \frac{1}{2}(1+y)(\ell + P_2^2 + Q_2^2)^2, \quad (\text{B.5})$$

while  $N$  and  $R$  become

$$N = \ell + P_1^2 + P_2^2 + Q_1^2 + Q_2^2$$

and

$$R = \ell + P_2^2 + Q_2^2.$$

### References

- [1] Nekhoroshev N N 1972 Action-angle variables and their generalizations. *Trans. Moscow Math. Soc.* **26** 180–98
- [2] Duistermaat J J 1980 On global action-angle coordinates *Commun. Pure Appl. Math.* **33** 687–706
- [3] Vũ Ngọc S 1999 Quantum monodromy in integrable systems *Commun. Math. Phys.* **203** 465–79
- [4] Guillemin V and Uribe A 1989 Monodromy in the quantum spherical pendulum *Commun. Math. Phys.* **122** 563–74
- [5] Cushman R H and Duistermaat J J 1988 The quantum mechanical spherical pendulum *Bull. Am. Math. Soc. (N. S.)* **19** 475–9
- [6] Nekhoroshev N N, Sadovskii D A and Zhilinskiĭ B I 2002 Fractional monodromy of resonant classical and quantum oscillators *Comptes Rendus Acad. Sci. Paris Ser. I* **335** 985–8
- [7] Nekhoroshev N N, Sadovskii D A and Zhilinskiĭ B I 2006 Fractional Hamiltonian monodromy *Annales Henri Poincaré* **7** 1099–211
- [8] Efstathiou K, Cushman R H and Sadovskii D A 2007 Fractional monodromy in the 1: – 2 resonance *Adv. Math.* **209** 241–73

- [9] Giacobbe A 2008 Fractional monodromy: parallel transport of homology cycles *Diff. Geom. Appl.* **26** 140–50
- [10] Hansen M S, Faure F and Zhilinskiĭ B I 2007 Fractional monodromy in systems with coupled angular momenta *J. Phys. A: Math. Theor.* **40** 13075
- [11] Cushman R H, Dullin H, Hanßmann H and Schmidt S 2007 The  $1:\pm 2$  resonance *Regular Chaotic Dyn.* **12** 642–63
- [12] Sugny D, Mardešić P, Pelletier M, Jebrane A and Jauslin H R 2008 Fractional Hamiltonian monodromy from a Gauss–Manin monodromy *J. Math. Phys.* **49** 042701–35
- [13] Broer H W, Efstathiou K and Lukina O V 2010 A geometric fractional monodromy theorem *Disc. Cont. Dyn. Sys. Ser. S* at press
- [14] Sadovskii D A and Zhilinskiĭ B I 2007 Hamiltonian systems with detuned  $1:1:2$  resonance: Manifestation of bidromy *Ann. Phys.* **322** 164–200
- [15] Colin de Verdière Y and Vũ Ngoc S 2003 Singular Bohr–Sommerfeld rules for 2D integrable systems *Ann. Sci. Éc. Norm. Sup.* **36** 1–55
- [16] Bolsinov A V and Fomenko A T 2004 *Integrable Hamiltonian systems: geometry, topology, classification* (Boca Raton, FL: Chapman & Hall/CRC)
- [17] Zung N T 1996 Symplectic topology of integrable Hamiltonian systems. I: Arnold–Liouville with singularities *Comput. Math.* **101** 179–215
- [18] Nekhoroshev N N 2007 Fractional monodromy in the case of arbitrary resonances *Sbornik: Math.* **198** 383–424
- [19] Nekhoroshev N N 2008 Fuzzy fractional monodromy and the section-hyperboloid *Milan J. Math.* **76** 1–14
- [20] Efstathiou K 2005 *Metamorphoses of Hamiltonian Systems with Symmetries (Lecture Notes in Mathematics vol 1864)* (Berlin: Springer)
- [21] Broer H W, Golubitsky M and Vegter G 2003 The geometry of resonance tongues: a singularity theory approach *Nonlinearity* **16** 1511–38
- [22] Broer H W, Holtman S J and Vegter G 2008 Recognition of the bifurcation type of resonance in mildly degenerate Hopf–Neimark–Sacker families *Nonlinearity* **21** 2463–82
- [23] Broer H W, Holtman S J, Vegter G and Vitolo R 2009 Geometry and dynamics of mildly degenerate Hopf–Neimark–Sacker families near resonance *Nonlinearity* **22** 2161–200
- [24] Efstathiou K, Sadovskii D A and Zhilinskiĭ B I 2007 Classification of perturbations of the hydrogen atom by small static electric and magnetic fields *Proc. R. Soc. A* **463** 1771–90
- [25] Radnović M and Rom-Kedar V 2008 Foliations of isoenergy surfaces and singularities of curves *Regular and Chaotic Dynamics* **13** 645–668
- [26] Cushman R H and Vũ Ngoc S 2002 Sign of the monodromy for Liouville integrable systems *Ann. H. Poincaré* **3** 883–94
- [27] Broer H W and Efstathiou K Uncovering fractional monodromy (in preparation)
- [28] Cushman R H and Bates L 1997 *Global Aspects of Classical Integrable Systems* (Basel: Birkhäuser)
- [29] Poston T and Stewart I 1978 *Catastrophe Theory and Its Applications* (London: Pitman)
- [30] Efstathiou K, Lukina O V and Sadovskii D A 2008 Most typical  $1:2$  resonant perturbation of the hydrogen atom by weak electric and magnetic fields *Phys. Rev. Lett.* **101** 253003
- [31] Assémat E, Efstathiou K, Joyeux M and Sugny D Fractional bidromy in the vibrational spectrum of HOCl (submitted)